

Modelling the Acquisition Geometry of a C-Arm Angiography System for 3D Reconstruction

Cristina Cañero^{1,2}, Eduardo Nofrerías³, Josefina Mauri³, and Petia Radeva^{1,2}

¹ Computer Vision Center, Edifici O Campus UAB, 08190 Cerdanyola, Spain.

² Computer Science Department, Universitat Autònoma de Barcelona, Spain

³ Hospital Universitari Germans Tries i Pujol, Badalona, Spain

`cristina@cvc.uab.es`

Abstract. This paper is concerned with the calibration of the intrinsic and extrinsic parameters of a X-ray angiographic system for 3D reconstruction of coronary vessel centerlines. We discuss whether the isocentric model is an accurate model for the movement of the C-arm, and analyse the assumptions made by this model. We propose a methodology which takes into account these facts and we propose for each model a calibration method. The calibration only needs a phantom that is commonly available by the physicians, since it is used to calibrate geometrical distortion. Then, we test the models with the calibration grid, as well as with a phantom imaged three months later. Experimental results show that by using the proposed models, it is not necessary neither a calibration nor a refinement at each acquisition.

1 Introduction

Digital X-ray angiography provides high quality images of coronary vessels. Assessing the percentage of stenosis and measuring the lesion length are applications with a great clinical interest. These measurements are obtained in clinical practice by comparing the size of the lesion to the width of the catheter appearance in the image disregarding the imprecision due to the perspective projection. In order to obtain reliable vessel measurements, a 3D reconstruction of vessels is a must. Other applications that need 3D reconstruction of vessels from angiography are the determination of optimal views [1] and the fusion of angiography with other medical image modalities like the intravascular ultrasound images to obtain a real volumetric 3D reconstruction of the vessel [2,3]. However, in order to obtain an accurate 3D reconstruction of a point, the acquisition geometry must be known with a high precision. In the angiographic frame, the model proposed by Dumay et al. in [1] is commonly used to predict the acquisition geometry. Nevertheless, authors in [4] state that the classical isocentric model could not satisfy the accuracy required, and thus proposes to use a variable isoaxis instead of a variable isocenter. Chen et al. in [5] proposes also the refining of the geometry for each acquisition for the same reason. Other authors, as Hoffman et al. in [6] propose to calibrate the imaging geometry using a phantom consisting on a cube with 12 lead markers attached on it at a known position. Although these

approaches provide a satisfying accuracy to the 3D reconstruction, they require a calibration at each acquisition, which becomes a time-consuming and tedious task in clinical practice.

We propose an improved model of the movement of the C-arm and an associated calibration technique, which only needs a phantom that is commonly available by the physicians. Experimental results show that the calibration must be performed only once. This fact highly simplifies the clinical application of diagnostic techniques involving 3D reconstruction from angiographies.

2 Materials and Methods

2.1 Extrinsic and Intrinsic Parameters Calibration

Given the general problem of pinhole camera calibration, Zhang in [7] proposes a technique to calibrate both the intrinsic and extrinsic parameters by using a planar pattern. This method can also be applied on the angiographic frame provided that the distance from the Image Intensifier (II) to the X-ray source remains constant for all views.

Zhang's Method. This technique only requires the camera (or angiography acquisition system) to observe a planar pattern shown at a few (at least two) different orientations. Either the camera or the planar pattern can be freely moved. The motion need not to be known. Thus, we can use the calibration grid used to estimate the geometrical distortion in [8] as calibration pattern.

Let $\tilde{\mathbf{m}} = [u, v, 1]^T$ be an augmented 2D point. A 3D point is denoted by $\widetilde{\mathbf{M}} = [X, Y, Z, 1]^T$. A camera is then modeled by the usual pinhole:

$$s\tilde{\mathbf{m}} = \mathbf{A} [\mathbf{R} \ \mathbf{t}] \widetilde{\mathbf{M}} \quad (1)$$

with

$$\mathbf{A} = \begin{bmatrix} \alpha & \gamma & u_0 \\ 0 & \beta & v_0 \\ 0 & 0 & 1 \end{bmatrix}$$

where s is an arbitrary scale factor, (\mathbf{R}, \mathbf{t}) the rotation and translation which relates world coordinates with camera coordinates, and \mathbf{A} is the camera intrinsic matrix, with (u_0, v_0) the coordinates of the principal point, α and β the scale factors and γ the skew factor.

In this method, the point is to assume that the model plane is on $Z = 0$ of the world coordinate system, so we can denote $\widetilde{\mathbf{M}} = [X, Y, 1]^T$. Therefore, a model point on world coordinates can be expressed in image coordinates by applying the homography \mathbf{H} :

$$s\tilde{\mathbf{m}} = \mathbf{H}\widetilde{\mathbf{M}} \quad \text{with} \quad \mathbf{H} = \mathbf{A} [\mathbf{r}_1 \ \mathbf{r}_2 \ \mathbf{t}]$$

where $\mathbf{r}_1, \mathbf{r}_2$ are the first and second columns of \mathbf{R} . \mathbf{H} is defined up to a scale factor and can be estimated for each view (see [7]).

Using the knowledge that \mathbf{r}_1 and \mathbf{r}_2 are orthonormal, we can define the following constraints for each view:

$$\begin{bmatrix} \mathbf{v}_{12}^T \\ (\mathbf{v}_{11} - \mathbf{v}_{22})^T \end{bmatrix} \mathbf{b} = \mathbf{0} \quad (2)$$

where

$$\mathbf{v}_{ij} = [h_{i1}h_{j1}, h_{i1}h_{j2} + h_{i2}h_{j1}, h_{i2}h_{j2}, h_{i1}h_{j3} + h_{i3}h_{j1}, h_{i2}h_{j3} + h_{i3}h_{j2}, h_{i3}h_{j3}]^T,$$

$$\mathbf{b} = [B_{11}, B_{12}, B_{22}, B_{13}, B_{23}, B_{33}]^T$$

and

$$\mathbf{B} = \lambda \mathbf{A}^{-T} \mathbf{A}^{-1} \equiv \lambda \begin{bmatrix} B_{11} & B_{12} & B_{13} \\ B_{21} & B_{22} & B_{23} \\ B_{31} & B_{32} & B_{33} \end{bmatrix}$$

For n images of the model plane, we can stack equations of (2) as:

$$\mathbf{Vb} = \mathbf{0} \quad (3)$$

Imposing the skewless constraint $\gamma = 0$, i.e., $[0, 1, 0, 0, 0, 0]\mathbf{b} = 0^1$ we can add an additional equation to (3). This allows us to obtain the remaining parameters by only using 2 views. The solution to 3 is the eigenvector of $\mathbf{v}^T \mathbf{v}$ associated with the smallest eigenvalue. Once \mathbf{B} is estimated, all camera intrinsic parameters can be computed as follows:

$$\begin{aligned} u_0 &= -\frac{B_{13}}{B_{11}} & v_0 &= -\frac{B_{23}}{B_{22}} \\ \lambda &= \frac{-B_{13}^2 B_{22} - B_{23}^2 B_{11} + B_{33} B_{22} B_{11}}{B_{22} B_{11}} \\ \alpha &= \sqrt{\frac{\lambda}{B_{11}}} & \beta &= \sqrt{\frac{\lambda}{B_{22}}} \end{aligned}$$

And the extrinsic parameters for each view are:

$$\begin{aligned} \mathbf{r}_1 &= \frac{\mathbf{A}^{-1} \mathbf{H}_1}{\|\mathbf{A}^{-1} \mathbf{H}_1\|}, & \mathbf{r}_2 &= \frac{\mathbf{A}^{-1} \mathbf{H}_2}{\|\mathbf{A}^{-1} \mathbf{H}_2\|}, \\ \mathbf{r}_3 &= \mathbf{r}_1 \times \mathbf{r}_2, & \mathbf{t} &= \frac{\mathbf{A}^{-1} \mathbf{H}_3}{\|\mathbf{A}^{-1} \mathbf{H}_1\|} \end{aligned}$$

For further details, see [7].

¹ In practice, we impose $[0, 1000, 0, 0, 0, 0]\mathbf{b} = 0$, since it makes somewhat stronger this constraint.

Using Zhang’s Method in the Angiographic Frame. The calibration pattern required by Zhang’s method can be easily constructed by printing a checker-box or a grid onto a paper and then fixing it to a rigid planar surface, for instance to a hard-covered book. Although this approach is not applicable when working with X-rays, we can use the same grid we used when calibrating Image Intensifiers’s distortion in [8] as calibration pattern. Thus, we propose to place the grid on the examination table, and acquire it by changing the anatomical angles for each view. Zhang’s method [7] can then be applied to obtain the intrinsic parameters, represented by matrix \mathbf{A} , and the extrinsic parameters, corresponding for each view i to matrices $\hat{\mathbf{R}}_i$ and $\hat{\mathbf{t}}_i$.

Nevertheless, this calibration is only valid for the acquired views, and we are interested in being able to compute the extrinsic parameters $\hat{\mathbf{R}}, \hat{\mathbf{t}}$ for any given configuration of the C-arm, determined by the anatomical angles α and β . To do that, we need to define a model of the movement of the C-arm, as the one proposed by Dumay et al. in [1], and then estimate the parameters of this model from the obtained $\hat{\mathbf{R}}_i$ and $\hat{\mathbf{t}}_i$ using Zhang’s method.

2.2 Modelling the Movement of the C-Arm

Modelling the movement of the C-arm means defining how to compute the extrinsic parameters \mathbf{R}, \mathbf{t} for any given configuration of the C-arm, determined by the anatomical angles α and β .

Dumay et al. defined in [1] the characteristic movements of a ceiling-mounted C-arm. First we will analyze this model and then introduce some modifications to improve its accuracy.

Dumay’s Model (M0). In the model proposed by Dumay et al. in [1], the fixed axis of rotation is directed horizontally and in longitudinal direction to the table. This axis is always projected ‘vertically’ in the images, i.e. its projection coincides with the y-axis on the image matrix. The projection of this fixed axis is therefore chosen as vector \mathbf{l} on the image plane. The axis perpendicular to \mathbf{l} on the image plane is denoted as \mathbf{k} and defined as:

$$\mathbf{k} = [0, -\cos \alpha, \sin \alpha]^T$$

The position of the plane, $\mathbf{C} = \|C\|\mathbf{c}$, where \mathbf{c} can be computed as:

$$\mathbf{c} = [\sin \beta, \sin \alpha \cos \beta, \cos \alpha \cos \beta]^T$$

The local reference system is chosen as a left-hand oriented orthogonal system, and thus the remaining axis \mathbf{l} is solved from:

$$\mathbf{l} = \mathbf{c} \times \mathbf{k}$$

From this model, we can define the extrinsic parameters \mathbf{R}', \mathbf{t}' as:

$$\mathbf{R} = \bar{\mathbf{R}} \quad \mathbf{t} = \bar{\mathbf{t}} \tag{4}$$

where

$$\bar{\mathbf{R}} = [\mathbf{k} \ \mathbf{l} \ \mathbf{c}]^T$$

and

$$\bar{\mathbf{t}} = [0, 0, \|C\|]^T$$

where $\|C\|$ is defined as the distance from the isocenter of rotation to the entrance screen of the image intensifier.

However, the model proposed by Dumay et al. makes the following assumptions:

- Vector \mathbf{l} coincides with the y axis on the image, and \mathbf{k} coincides with the x axis on the image.
- The imaging equipment is properly aligned and thus the central beams intersect at the isocenter of rotation.
- The rotation and angulation axes do intersect, i.e. there is an isocenter.
- The rotation and angulation axes are perfectly orthogonal.
- The central beam is orthogonal to the angulation axis.

We will analyse each assumption and, if necessary, we will define a model for each case.

Model with Image Rotation (M1). Vector \mathbf{l} and \mathbf{k} may not coincide with the y axis and x axis on the image, respectively, since the Image Intensifier (II) introduces a distortion with a rotational effect. Our undistortion method presented in [8] fixed image rotation and other distortions, even the orientation-dependent ones, by estimating the distortion model from the anatomical angles. Nevertheless, and since the ground truth orientation of the image is unknown, the resulting undistorted image will be in general rotated from the ideal undistorted one. Moreover, rotation and angulation axis of the isocentric model could be not aligned with the ideal image.

Therefore, image rotation can stem both from II's distortion and from image misalignment. For simplicity, we will combine both rotations on a unique rotation matrix $\mathbf{R}_d = R_z(\theta)$, which will be applied before projecting. Since this rotation is not in general performed on the origin of coordinates, we should add a displacement vector $\mathbf{t}_d = [d_x, d_y, 0]^T$ after rotating². Thus, the extrinsic parameters defined by this model are:

$$\mathbf{R} = \mathbf{R}_d \bar{\mathbf{R}} \quad \mathbf{t} = \mathbf{R}_d \bar{\mathbf{t}} + \mathbf{t}_d$$

since $\bar{\mathbf{t}}$ is a displacement among z axis, matrix \mathbf{R}_d has no effect on it, and thus:

$$\mathbf{R} = \mathbf{R}_d \bar{\mathbf{R}} \quad \mathbf{t} = \bar{\mathbf{t}} + \mathbf{t}_d \quad (5)$$

² Although the rotation related to angulation and rotation angles misalignment is performed before projecting and the one related to II distortion is performed after, it is very easy to show that we can do this simplification.

Non Intersecting Central Beams. If the imaging equipment is not properly aligned, the central beam does not intersect the isocenter of rotation, i.e., the isocenter is also displaced (ϵ_x, ϵ_y) from the central beam in the plane perpendicular to it. We assume that this displacement is constant for all views. Although this situation is possible, it can be modelled with the previous model, since parameters d_x, d_y can compensate this effect. Therefore, we will not define a model for this situation.

Non Intersecting Rotation Axis (M2). If the two rotation axis do not intersect, the isocentric model is not valid. Instead, we should define a model with a displacement between the two rotation axis and perpendicular to both. Since rotation, defined by α angle, is performed around the y axis and angulation around the x axis, this displacement will be along the z axis after α rotation. Let ϵ be this displacement, then we can define the following model for the external parameters:

$$\begin{aligned} \mathbf{R} &= \mathbf{R}_d R_x(\beta) R_y(\alpha) \\ \mathbf{t} &= \bar{\mathbf{t}} + \mathbf{t}_d + \mathbf{R}_d(\mathbf{I} - R_x(\beta))[0; 0; \epsilon]^T \end{aligned} \quad (6)$$

where $R_y(\alpha)$ corresponds to the rotation and $R_x(\beta)$ to the angulation³.

Non Orthogonal Rotation Axes (M3). Although the rotation axes are expected to be orthogonal, perfect orthogonality is hard to achieve, and thus the angulation axis will be slightly rotated from its ideal position. Moreover, the anatomical angles could be measured as $\alpha' = \alpha + \Delta\alpha$ and $\beta' = \beta + \Delta\beta$. This fact would have an equivalent effect on the extrinsic parameters as the non orthogonality of the rotation axes. Therefore, we introduce the rotation matrix \mathbf{R}_p in our model, and the extrinsic parameters will be:

$$\begin{aligned} \mathbf{R} &= \mathbf{R}_d R_x(\beta) \mathbf{R}_p R_y(\alpha) \\ \mathbf{t} &= \bar{\mathbf{t}} + \mathbf{t}_d + \mathbf{R}_d(\mathbf{I} - R_x(\beta) \mathbf{R}_p)[0; 0; \epsilon]^T \end{aligned} \quad (7)$$

Central Beam Non Orthogonal to Angulation Axis (M4). In theory, the central beam should be perpendicular to the angulation axis. Nevertheless, this may not be true, and hence we introduce matrix \mathbf{R}_b in the model. This matrix will describe the rotation between the central beam and the ideal one, which is perpendicular to the angulation axis. Thus, the model will be **M3**, but

³ Note that if we compute $R_x(\beta)R_y(\alpha)$ we will not obtain $\bar{\mathbf{R}}$, but $\bar{\mathbf{R}}\mathbf{R}_a$, where

$$\mathbf{R}_a = \begin{bmatrix} 0 & -1 & 0 \\ 1 & 0 & 0 \\ 0 & 0 & 1 \end{bmatrix}$$

This is not important to obtain a 3D reconstruction, nor have effect when calibrating.

replacing \mathbf{R}_d by \mathbf{R}_b . Thus, we obtain the following expression for the extrinsic parameters:

$$\begin{aligned} \mathbf{R} &= \mathbf{R}_b R_x(\beta) \mathbf{R}_p R_y(\alpha) \\ \mathbf{t} &= \bar{\mathbf{t}} + \mathbf{t}_d + \mathbf{R}_b(\mathbf{I} - R_x(\beta) \mathbf{R}_p)[0; 0; \epsilon]^T \end{aligned} \tag{8}$$

2.3 Calibrating the C-Arm’s Movement Model

Zhang’s approach assumes that the world coordinate system is placed on the calibration pattern. This coordinate system does not in general coincide with the rotation and angulation axes. Thus, there is a rigid transform, represented by $\mathbf{R}_w, \mathbf{t}_w$ between the two coordinate systems. If the model is exact and well calibrated, the extrinsic parameters $\mathbf{R}_i, \mathbf{t}_i$ predicted by the model and the matrices $\hat{\mathbf{R}}_i, \hat{\mathbf{t}}_i$, estimated using Zhang’s approach, should fulfill the following:

$$\hat{\mathbf{R}}_i = \mathbf{R}_i \mathbf{R}_w \quad \hat{\mathbf{t}}_i = \mathbf{R}_i \mathbf{t}_w + \mathbf{t}_i \tag{9}$$

Our aim is thus to estimate the parameters of each model and the rigid transform $\mathbf{R}_w, \mathbf{t}_w$, which fits the best the estimated matrices $\hat{\mathbf{R}}_i, \hat{\mathbf{t}}_i$ using Zhang’s approach to the ideal matrices $\mathbf{R}_i, \mathbf{t}_i$ of each model.

M0 Calibration. The parameters to be estimated are $\mathbf{R}_w, \mathbf{t}_w$ and $\|C\|$. Using equation (4) and (9), we can state the following:

$$\hat{\mathbf{R}}_i = \bar{\mathbf{R}}_i \mathbf{R}_w \quad \hat{\mathbf{t}}_i = \bar{\mathbf{R}}_i \mathbf{t}_w + \bar{\mathbf{t}}_i$$

For each view i , we can compute an estimation of \mathbf{R}_w as:

$$\mathbf{R}_w^i = \bar{\mathbf{R}}_i^T \hat{\mathbf{R}}_i$$

The estimated \mathbf{R}_w can then be assumed to be the mean of \mathbf{R}_w^i . To estimate the mean of a set of rotations, we use the approach proposed in [9].

On the other hand, for each view we can define the following set of linear constraints:

$$[\bar{\mathbf{R}}_i [0, 0, 1]^T] \begin{bmatrix} \mathbf{t}_w \\ \|C\| \end{bmatrix} = \hat{\mathbf{t}}_i$$

These constraints can be stacked to construct an overdetermined linear system of equations, which can be resolved by applying any linear least squares approach. Since there are 4 independent unknown variables - namely, \mathbf{t}_w and $\|C\|$ -, we need at least 2 views.

M1 Calibration. Using equations (5) and (9), we obtain:

$$\hat{\mathbf{R}}_i = \mathbf{R}_d \bar{\mathbf{R}}_i \mathbf{R}_w \quad \hat{\mathbf{t}}_i = \mathbf{R}_d \bar{\mathbf{R}}_i \mathbf{t}_w + \bar{\mathbf{t}}_i + \mathbf{t}_d \tag{10}$$

Note that $\mathbf{R}_w, \mathbf{t}_w, \mathbf{R}_d, \mathbf{t}_d$ and $\bar{\mathbf{t}}_i$ should be constant for all views.

First, we need to estimate \mathbf{R}_d . Given two views i, j with $i \neq j$, we can compute the following:

$$\hat{\mathbf{R}}_i \hat{\mathbf{R}}_j^T = \mathbf{R}_d \mathbf{R}_i \mathbf{R}_w \mathbf{R}_w^T \mathbf{R}_j^T \mathbf{R}_d^T$$

and using that \mathbf{R}_w is a rotation matrix and thus $\mathbf{R}_w \mathbf{R}_w^T = \mathbf{I}$, we can state that:

$$\hat{\mathbf{R}}_i \hat{\mathbf{R}}_j^T = \mathbf{R}_d \mathbf{R}_i \mathbf{R}_j^T \mathbf{R}_d^T$$

Since \mathbf{R}_d is uniquely determined by the angle θ , this non-linear system is very easy to solve by applying any standard non-linear least squares approach. In this work, we have applied the Gauss-Newton method to estimate θ . To construct the error function, we have used the metric proposed in [9] to compute the distance between two rotations.

Once we have an estimate of \mathbf{R}_d , we can proceed to estimate the other parameters. First, for each view i , we can compute an estimate of \mathbf{R}_w as:

$$\mathbf{R}_w^i = \bar{\mathbf{R}}_i^T \mathbf{R}_d^T \hat{\mathbf{R}}_i$$

The estimated \mathbf{R}_w can then be assumed to be the mean of \mathbf{R}_w^i , which can be computed as proposed in [9].

Second, for each view we can define the following set of linear constraints:

$$[\mathbf{R}_d \mathbf{R}_i \mathbf{I}] \begin{bmatrix} \mathbf{t}_w \\ \mathbf{t}_i + \mathbf{t}_d \end{bmatrix} = \hat{\mathbf{t}}_i$$

where

$$\mathbf{t}_i + \mathbf{t}_d = [d_x, d_y, \|C\|]^T$$

These constraints can be stacked to construct an overdetermined linear system of equations, which can be resolved by applying any linear least squares approach. Since there are 6 independent unknown variables - namely, \mathbf{t}_w , d_x , d_y and $\|C\|$ -, we need at least 2 views.

The obtained parameters θ , \mathbf{R}_w , \mathbf{t}_w , d_x , d_y and $\|C\|$ can then be refined by using a non-linear least squares minimization method using as error function the sum of the squared distances between the detected intersection points on the images and the predicted ones using the model.

M2 Calibration. Using equations (6) and (9), we obtain the following relation:

$$\begin{aligned} \hat{\mathbf{R}}_i &= \mathbf{R}_d R_x(\beta_i) R_y(\alpha_i) \mathbf{R}_w \\ \hat{\mathbf{t}}_i &= \mathbf{R}_d R_x(\beta_i) R_y(\alpha_i) \mathbf{t}_w + \bar{\mathbf{t}}_i + \mathbf{t}_d + \\ &\quad \mathbf{R}_d (\mathbf{I} - R_x(\beta_i)) [0, 0, \epsilon]^T \end{aligned}$$

To estimate the parameters of the model, we first estimate θ by using the non-linear approach used to calibrate the previous model, replacing $\hat{\mathbf{R}}_i$ by

$R_x(\beta_i)\hat{R}_y(\alpha_i)$. Once we have an estimate of θ , and thus of \mathbf{R}_d , we can define the following set of linear constraints for each view i :

$$[\mathbf{R}_d R_x(\beta_i) R_y(\alpha_i) \mathbf{b} \mathbf{I}] \begin{bmatrix} \mathbf{t}_w \\ \epsilon \\ d_x \\ d_y \\ \|C\| \end{bmatrix} = \hat{\mathbf{t}}_i$$

where

$$\mathbf{b} = \mathbf{R}_d(\mathbf{I} - R_x(\beta_i))[0, 0, 1]^T$$

These constraints can be stacked to construct an overdetermined linear system of equations, which can be resolved by applying any linear least squares approach. Since there are 7 independent unknown variables - namely, \mathbf{t}_w , ϵ , d_x , d_y and $\|C\|$ -, we need at least 3 views.

Finally, the obtained parameters θ , \mathbf{R}_w , \mathbf{t}_w , ϵ , d_x , d_y and $\|C\|$ can be refined by using a non-linear least squares minimization method to fit the predicted positions of the intersection points of the grid to the detected ones on the images, as we have done with model **M1**.

M3 Calibration. Using equations (7) and (9), we can state the following:

$$\begin{aligned} \hat{\mathbf{R}}_i &= \mathbf{R}_d R_x(\beta) \mathbf{R}_p R_y(\alpha) \mathbf{R}_w \\ \hat{\mathbf{t}}_i &= \mathbf{R}_d R_x(\beta) \mathbf{R}_p R_y(\alpha) \mathbf{t}_w + \bar{\mathbf{t}}_i + \mathbf{t}_d + \mathbf{R}_d(\mathbf{I} - R_x(\beta) \mathbf{R}_p)[0, 0, \epsilon]^T \end{aligned}$$

Since we have not found a closed form solution to estimate the parameters of this model, we propose to fit model **M2** and then use the obtained parameters θ , \mathbf{R}_w , \mathbf{t}_w , ϵ , d_x , d_y and $\|C\|$ and the added $\mathbf{R}_p = \mathbf{I}$ as starting guess for a non-linear minimization procedure. As before, the error functional to be minimized will be the squared distance between the predicted positions of the intersections on the grid and the detected ones on the images.

M4 Calibration. Using equations (8) and (9), we can obtain the following expression for matrices $\hat{\mathbf{R}}_i$, $\hat{\mathbf{t}}_i$:

$$\begin{aligned} \hat{\mathbf{R}}_i &= \mathbf{R}_b R_x(\beta) \mathbf{R}_p R_y(\alpha) \mathbf{R}_w \\ \hat{\mathbf{t}}_i &= \mathbf{R}_b R_x(\beta) \mathbf{R}_p R_y(\alpha) \mathbf{t}_w + \bar{\mathbf{t}}_i + \mathbf{t}_d + \mathbf{R}_b(\mathbf{I} - R_x(\beta) \mathbf{R}_p)[0, 0, \epsilon]^T \end{aligned}$$

To estimate the parameters of this model, we can start with the parameter estimate for model **M3** as initial guess (with $\mathbf{R}_b = \mathbf{R}_d$), and run a non-linear minimization procedure. Again, the error function will be the squared distance between the positions of the intersections on the grid predicted by the model and the detected ones on the images.

3 Experimental Results

The experimental results presented in this work were performed using a SIEMENS Cathcor 3.3 C-arm angiography acquisition system in the University Hospital "Germans Trias i Pujol" (Badalona, Spain). This system is laterally mounted instead of ceiling-mounted, and thus we must replace α by $-\alpha$ and β by $-\beta$ in the formulae proposed. Figure 1 illustrates how anatomical angles are defined in our system.

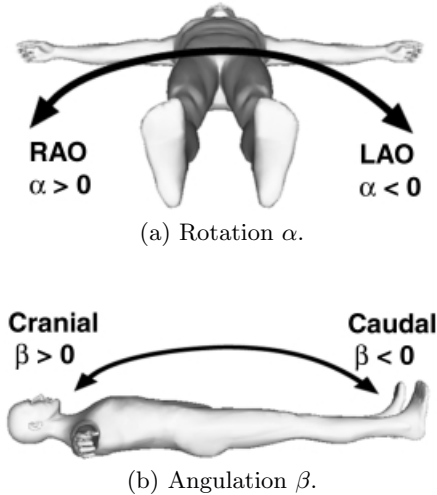


Fig. 1. Anatomic angles for a laterally mounted SIEMENS Cathcor 3.3 C-arm, which define the orientation of the detector.

3.1 Zhang's Calibration on a C-Arm Angiographer from SIEMENS

We have acquired the grid for different positions of the C-arm, namely for $\alpha \in \{-30, -15, -5, 0, 5, 15, 30\}$ and $\beta \in \{-20, -15, -10, 0, 10, 15, 20\}$. First, we have detected the intersections for each view i , thus obtaining $\hat{\mathbf{u}}_i, \hat{\mathbf{v}}_i$, the distorted positions on the image of the intersection points on the grid, and $\mathbf{x}_i, \mathbf{y}_i$, the real positions in world coordinates (in cm). After, we have applied the undistortion method proposed in [8] to obtain the undistorted coordinates $\mathbf{u}_i, \mathbf{v}_i$. Third, we have applied Zhang's method to $\mathbf{u}_i, \mathbf{v}_i$ and $\mathbf{x}_i, \mathbf{y}_i$, obtaining matrices \mathbf{A} , $\hat{\mathbf{R}}_i$ and $\hat{\mathbf{t}}_i$. Finally, we have computed the following expression for each view i and detected position j :

$$E_{ij} = \begin{bmatrix} u_{ij} \\ v_{ij} \end{bmatrix} - \mathbf{A}[\mathbf{R}_i - \mathbf{t}_i] \begin{bmatrix} x_{ij} \\ y_{ij} \\ \mathbf{0} \\ \mathbf{1} \end{bmatrix}$$

The standard deviation of E_{ij} was of 0.13 pixels, and the maximum value of $\|E_{ij}\|$ was of 0.8 pixels.

3.2 Accuracy of the Proposed Models

The aim of this experiment is to determine which model fits the best to the real movement of the C-arm. In order to do that, we have first divided the acquired views of the previous experiment in two sets: the calibration and the test set. Then, we have estimated the parameters of each model for each view of the calibration set, using the estimated $\hat{\mathbf{R}}_i$ and $\hat{\mathbf{t}}_i$ of the previous experiment. Finally, and for each model, we have computed the following expression for each view i and position j :

$$E_{ij} = \begin{bmatrix} u_{ij} \\ v_{ij} \end{bmatrix} - \mathbf{A}[\mathbf{R}_i^k \mathbf{t}_i^k] \begin{bmatrix} x_{ij} \\ y_{ij} \\ \mathbf{0} \\ \mathbf{1} \end{bmatrix}$$

where matrices \mathbf{R}_i^k and \mathbf{t}_i^k are the predicted extrinsic parameters for view i and model \mathbf{Mk} , using the estimated parameters. Table 1 shows the results obtained.

Table 1. Displacement E (in pixels) between the detected intersection points on the grid and predicted positions for each model, computed both for calibration and test sets.

	Calibration		Test	
	std(E)	max $\ E\ $	std(E)	max $\ E\ $
M0	6.81	33.38	5.63	23.00
M1	1.80	10.15	1.85	9.77
M2	1.98	13.14	1.96	11.07
M3	1.08	8.49	1.00	4.77
M4	0.91	5.39	0.86	5.44

From these results, we can state that the model which better fits is **M4**. Note the large maximal errors introduced by model **M0**. Since the distance between wires on the grid is of 1cm and the projected gap on the image measures a mean of 40 pixels, an error of 30 pixels is very important.

3.3 3D Reconstruction of a Phantom

Three months after the calibration date, we have acquired a phantom consisting on a wavy wire, simulating a vessel. The wire was imaged for different views, namely, for $\alpha \in [30^\circ, 0^\circ, -30^\circ]$ and $\beta \in [15^\circ, 0^\circ, -15^\circ]$.

We have then estimated for each model the corresponding extrinsic parameters for all views by using the calibration performed in the previous experiment.

Table 2. Here D is the distance from each projected point of the curve to the nearest position on the image corresponding to wire. $|D|$ is the mean of distance D for all views, and $\max|D_i|$ is the maximum value of the mean distance computed for each view. All values are in pixels.

Model	Ignoring distortion		Including distortion	
	$ D $	$\max D_i $	$ D $	$\max D_i $
M0	4.0	7.9	3.4	7.5
M1	0.6	1.5	0.6	1.4
M2	0.5	1.5	0.5	1.4
M3	0.4	0.9	0.2	0.5
M4	0.3	0.6	0.1	0.3

For the intrinsic parameters, it must be noted that the distance from the X-ray source to the Image Intensifier's screen was different from the calibration acquisitions, i.e. whereas when calibrating it was of 95cm, in this experiment was of 100cm. Therefore, to determine the intrinsic parameters, i.e. matrix \mathbf{A} , we have recomputed components A_{11} and A_{22} as $A_{11} = 100/95\hat{A}_{11}$ and $A_{22} = 100/95\hat{A}_{22}$, where $\hat{\mathbf{A}}$ is the matrix estimated using Zhang's method.

From each model, we have reconstructed the phantom using a biplane snake (for a description of biplane snakes, see [10]) and views $[\alpha_1 = 30^\circ, \beta_1 = 0^\circ]$ and $[\alpha_2 = -30^\circ, \beta_2 = 0^\circ]$. We have done two reconstructions: ignoring the distortion introduced by the Image Intensifier, and using the distortion/undistortion model proposed in [8].

Finally, we have projected the reconstructed curve on the other views, to see whether the projection of the curve fits the image. Figure 3.3 shows the obtained curve projected for a view with $\alpha = 0$ and $\beta = 15$, for each model. Note that the curve fits pretty accurately for models **M3** and **M4**. Numerical results are presented in table 2.

4 Discussion

We have proposed a method to calibrate the extrinsic and intrinsic parameters of a C-arm by using a phantom which is commonly available by the physicians, since it is the one used to calibrate geometrical distortion.

Then, we have discussed whether the isocentric model is an accurate model for the movement of the C-arm. In particular, we question whether the rotation axis and the angulation axis do intersect, if there is not a perfect orthogonality between the two axes, and also if the central beam is orthogonal to the angulation axis. We have therefore proposed models which take into account these facts, and estimated its parameters by using a calibration grid. Then, we have tested the models with a phantom imaged three months later. Experimental results lead us to believe that our models perform better than the traditional isocentric model. In particular, they conduct us to select model **M4** as the model to be used for 3D reconstruction purposes. Moreover, the accuracy obtained in the experiments

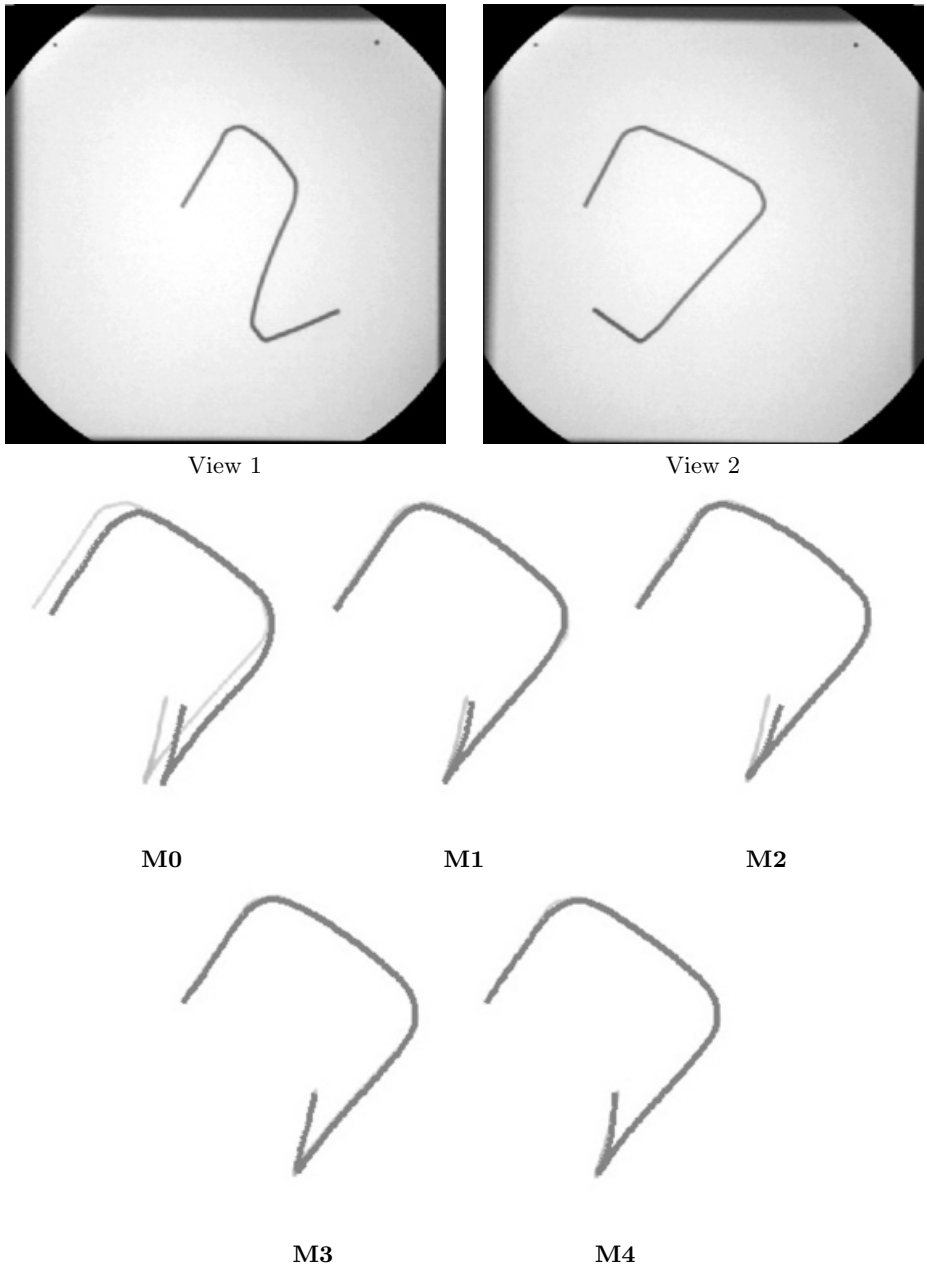


Fig. 2. Projection of the reconstructed 3D curve (dark) using each model at $\alpha = 0, \beta = 15$. The curve was obtained from views $\alpha = 30, \beta = 0$ (view 1) and $\alpha = -30, \beta = 0$ (view 2). Geometrical distortion introduced by the Image Intensifier was taken into account.

encourages us to state that by using model **M4**, it shall not be necessary a calibration nor a refinement at each acquisition, as proposed in [4,5,6], but only a periodic calibration. This fact is very important, since it highly simplifies the clinical application of diagnostic techniques involving 3D reconstruction from angiographies.

Acknowledgments. This work was supported in part by the catalonian *Departament d'Universitats, Recerca i Societat de la Informació* under the grant 1999FI 00753 APTIND CVC and by the spanish *Ministerio de Ciencia y Tecnología* under the projects TIC2000-1635-C04-04 and TIC2000-0399-C02-01.

References

1. Dumay, A., Reiber, J., Gerbrands, J.: Determination of optimal angiographic viewing angles: Basic principles and evaluation study. *IEEE Transactions on Medical Imaging* **13** (1994)
2. Pujol, O., Cañero, C., Radeva, P., Toledo, R., Saludes, J., Gil, D., Villanueva, J., Mauri, J., García, B., Gómez, J., Cequier, A., Esplugas, E.: Three-dimensional reconstruction of coronary tree using intravascular ultrasound images. In: *Computers in Cardiology*. (1999) 265–268
3. Wahle, A., Prause, G., DeJong, S., Sonka, M.: Geometrically correct 3-D reconstruction of intravascular ultrasound images by fusion with biplane angiography - methods and validation. *IEEE Transactions on Medical Imaging* **18** (1999)
4. Wahle, A., Wellnhofer, E., Mugaragu, I., Sauer, H., Oswald, H., Fleck, E.: Assessment of diffuse coronary artery disease by quantitative analysis of coronary morphology based upon 3-D reconstruction from biplane angiograms. *IEEE Transactions on Medical Imaging* **14** (1995) 230–241
5. Chen, S., Metz, C.: Improved determination of biplane imaging geometry from two projection images and its application to three-dimensional reconstruction of coronary arterial trees. *Medical Physics* **25** (1997) 633–654
6. Hoffmann, K., Williams, B., Esthappan, J., Chen, S.Y., Carroll, J., Harauchi, J., Doerr, V., Kay, G., Eberhardt, A., Overland, M.: Determination of 3D positions of pacemaker leads from biplane angiographic sequences. *Medical Physics* **24** (1997) 1854–1862
7. Zhang, Z.: A flexible new technique for camera calibration. *IEEE Transactions on Pattern Analysis and Machine Intelligence* **22** (2000) 1330–1334
8. Cañero, C., Vilariño, F., Mauri, J., Radeva, P.: Predictive (un)distortion model and 3D reconstruction by biplane snakes. *IEEE Transactions on Medical Imaging*, to appear (2002)
9. Pennec, X.: Computing the mean of geometric features. Application to the mean rotation. Technical report, INRIA (1998) Available at <http://www-sop.inria.fr/rapports/sophia/RR-3371.html>.
10. Cañero, C., Radeva, P., Toledo, R., Villanueva, J., Mauri, J.: 3D curve reconstruction by biplane snakes. In: *Proceedings of International Conference on Pattern Recognition*. Volume 4. (2000) 563–566